Cross-correlation task-related component analysis (xTRCA) for enhancing evoked and induced responses of event-related potentials

Hirokazu Tanaka [a*] and Makoto Miyakoshi [b]

a. School of Information Science
Japan Advanced Institute of Science and Technology
1-1 Asahidai, Nomi, Ishikawa 923-1211, Japan

b. Swartz Center for Computational Neuroscience
Institute of Neural Computation
University of California San Diego
9500 Gilman Drive # 0559
La Jolla CA 92093-0559, U.S.A.

* Corresponding author

Text page: 48
Abstract: 238 words

Abbreviated Title: Cross-correlation task-related component analysis (xTRCA)

Corresponding author:
Hirokazu Tanaka
Email: hirokazu@jaist.ac.jp
Tel: +81-761-51-1226 Fax: +81-761-51-1149

Key words: EEG data analysis; Multivariate analysis; Trial-by-trial reproducibility; Generalized eigenvalue problem; Matrix perturbation; Woody's method; Evoked response; Induced response

ABSTRACT

We propose an analysis method that extracts trial-reproducible (i.e., recurring) event-related spatiotemporal EEG patterns by optimizing a spatial filter as well as trial timings of task-related components in the time domain simultaneously in a unified manner. Event-related responses are broadly categorized into evoked and induced responses, but those are analyzed commonly in the time and the time-frequency domain, respectively. To facilitate a comparison of evoked and induced responses, a unified method for analyzing both evoked and induced responses is desired. Here we propose a method of cross-correlation task-related component analysis (xTRCA) as an extension of our previous method. xTRCA constructs a linear spatial filter and then optimizes trial timings of single trials based on trial reproducibility as an objective function. The spatial filter enhances event-related responses, and the temporal optimization compensates trial-by-trial latencies that are inherent to ERPs. We first applied xTRCA to synthetic data of induced responses whose phases varied from trial to trial, and found that xTRCA could realign the induced responses by compensating the phase differences. We then demonstrated with mismatch negativity data that xTRCA enhanced the event-related-potential waveform observed at a single channel. Finally, a classification accuracy was improved when trial timings were optimized by xTRCA, suggesting a practical application of the method for a brain computer interface. We conclude that xTRCA provides a unified framework to analyze and enhance event-related evoked and induced responses in the time domain by objectively maximizing trial reproducibility.

1. Introduction

EEG data are often analyzed by aligning event-related potentials (ERPs) to event onsets such as stimulus presentation and motor outputs and taking an average across trials either in the time or the time-frequency domain (Cohen, 2014; Luck, 2014). There are two broad classes of EEG responses, evoked and induced (Galambos, 1992; Cohen, 2014). Evoked potentials are both time-locked and phase-locked to event onsets and are obtained by calculating an average across trials in the time domain, assuming that trial-by-trial variability results from additive noises, which are canceled by temporal averaging (Luck, 2014). In contrast, induced potentials are similarly time-locked but not phases-locked from trial to trial, so they cancel out each other after averaging in the time domain (Makeig, 1993). Induced potentials have been analyzed in the time-frequency domain using a wavelet transform, since signal powers are positive definite and never cancel out by trial averaging.

Even though a wavelet analysis works for induced response analysis, it does not substitute the ERP waveform analysis in the time domain for the following reasons; 1) The concept of temporal resolution in wavelet analysis is different from that in ERP waveform analysis — wavelet analysis uses a kernel function and a sliding window that are often determined arbitrarily; 2) Although wavelet transform is generally applied to induced ERP data analysis, the nature of phase jitter, such as distribution, cannot be explicitly calculated; and 3) Rich knowledge of conventional ERP literature becomes unavailable when interpreting wavelet analysis results. Hence, we expect it to be useful if an ERP waveform analysis in the time domain is available for induced responses as well.

The proposed method in this study integrates two conventional approaches to enhance ERP waveforms either in spatial or temporal domain. First, the spatial approach exploits statistics of multiple time series measured over the scalp to improve the reproducibility of signals from trial to trial. xDAWN decomposes measured EEG time series into a component that occurs every trial and was demonstrated to enhance P300 wave forms (Rivet et al., 2009). Reliable component analysis computes a weighted sum of Fourier coefficients at selected frequencies and was shown to extract reliable components from SSVEP data set (Dmochowski et al., 2015). We independently proposed task-related component analysis (TRCA), which finds a weighted sum of multi-channel inputs that maximizes trial reproducibility of a signal using a linear spatial filter (Tanaka et al., 2013, 2014). These methods differ in their detailed formulations and implementations but share an assumption that trial-reproducible components are embedded within multiple time series of observed EEG data.

The temporal approach, on the other hand, compensates trial timings by shifting time windows of trials so that trial-by-trial variability of latency is minimized (Woody, 1967; Jaskowski and Verleger, 1999; Cabasson and Meste, 2008; Ouyang et al., 2011; Thompson et al., 2013; Gips et al., 2017; Da Pelo et al., 2018). The seminal work by Woody finds ERP latency by computing a cross correlation of a single-trial time course and a template and then searches for a time shift of that trial that maximizes the cross correlation (Woody, 1967). Woody's original method has been revisited in more recent papers in which trial-by-trial variation of ERP latency is compensated by a maximum likelihood method, Markov-chain Monte-Carlo method, or genetic algorithm (Jaskowski and Verleger, 1999; Thompson et al., 2013; Gips

et al., 2017). Whereas Woody's method and its extensions have conventionally been applied to an enhancement of evoked potentials in single channels, latency compensation is expected to help induced potentials align for the case of multivariate analysis in the time domain, thereby allowing trial averaging in the time domain.

In this study, we propose cross-correlation task-related component analysis (xTRCA) that integrates the spatial and temporal approaches reviewed above. With given trial timings, a spatial filter is constructed by maximizing trial reproducibility, and with a given spatial filter, trial timings are optimized to increase trial reproducibility. Our proposed method, therefore, optimizes a spatial filter and trial timings based on a single objective of trial reproducibility, handling induced and evoked responses in a unified manner. It is known that even evoked potentials have intrinsic latency jitter across trials, sessions, and subjects (Sklare and Lynn, 1984; Segalowitz and Barnes, 1993; Pekkonen et al., 1995; Corsi-Cabrera et al., 2007; Huffmeijer et al., 2014), so our method is expected to enhance ERPs of evoked responses. In the following sections, xTRCA is first validated using simulated data of induced responses and is then applied to mismatch negativity data. Finally, we demonstrate that xTRCA improves a performance for a classification task between two conditions, suggesting a possible application for brain-computer interfaces.

2. Method

2.1. Task-related component analysis (TRCA)

Before formulating xTRCA, we here provide a brief review of TRCA. Figure 1 provides a schematic

explanation of TRCA. Assume that we have *n*-channel data of length *T*, denoted by $\mathbf{X} \in \mathbb{R}^{n \times T}$ (continuous data), and that there are *K* experimental trials with known latencies of event onsets. Data points within *k*-th trial is denoted by $\mathbf{X}^{(k)} \in \mathbb{R}^{n \times \tau}$ (time-windowed data) where τ is the number of data points in a trial (i.e., trial length) (Figure 1A). The time windows of the trials are defined by event onsets and are denoted by $\mathbf{t} = \left(t_1, \cdots, t_K\right)^{\mathrm{T}} \in \mathbb{R}^K$. The vector $\mathbf{t}$ is referred to as a timing vector. TRCA extracts a component by taking a weighted sum of all channels $\mathbf{y} = \mathbf{w}^\top \mathbf{X} \in \mathbb{R}^{1 \times T}$ with a spatial filter $\mathbf{w} \in \mathbb{R}^n$ so that the task-related component $\mathbf{y}$ is maximally reproducible from trial to trial. A time series from each channel is normalized to zero mean and unit variance over the whole duration. Let us define the covariance matrix of time-windowed data of all possible pairs of k-th and ℓ-th trials defined as

$$\mathbf{S} = \frac{1}{K\left(K-1\right)\tau} \sum_{k \neq \ell}^{K} \mathbf{X}^{(k)} \mathbf{X}^{(\ell)\top} \in \mathbb{R}^{n \times n}, \tag{1}$$

and the covariance matrix of continuous data defined as

$$\mathbf{Q} = \frac{1}{T} \mathbf{X}\mathbf{X}^\top \in \mathbb{R}^{n \times n}. \tag{2}$$

In Eq. (1), the summation is taken over all possible trial pairs of *k*-th and *l*-th trials, and this definition of the matrix **S** contains *K*(*K*-1) summations. By noting an equivalent but alternative definition of the matrix **S**,

$$\mathbf{S} = \frac{K}{\left(K-1\right)\tau} \left(\mathbf{U}\mathbf{U}^\top - \frac{1}{K}\mathbf{V} \right) \in \mathbb{R}^{n \times n}, \tag{3}$$

where the matrices **U** and **V** are defined as

$$\begin{aligned}\mathbf{U} &= \frac{1}{K}\sum_{k=1}^{K}\mathbf{X}^{(k)} \in \mathbb{R}^{n\times\tau} \\ \mathbf{V} &= \frac{1}{K}\sum_{k=1}^{K}\mathbf{X}^{(k)}\mathbf{X}^{(k)\top} \in \mathbb{R}^{n\times n}\end{aligned}. \tag{4}$$

This definition involves only *K* summations and accelerates the computation of the matrix S, especially when the number of trials *K* is large. Note that because of the $-\frac{1}{K}\mathbf{V}$ term in the parentheses, the matrix is not positive semidefinite hence it can contain negative eigenvalues. As explained below, TRCA uses the second order statistics of the **S** and **Q** matrices, so we assume that the covariance matrices capture the spatiotemporal dynamics of ERPs and are stationary over time.

Given the **S** and **Q** matrices, the problem of TRCA is now formulated as:

$$\text{maximize } \mathbf{w}^{\top}\mathbf{S}\mathbf{w} \text{ subject to } \mathbf{w}^{\top}\mathbf{Q}\mathbf{w} = 1. \tag{5}$$

as illustrated in Figure 1B. Importantly, this spatial filter **w** guarantees maximum covariance between $\mathbf{y}^{(k)}$ of *k*-th trial and $\mathbf{y}^{(\ell)}$ of *l*-th trial, hence **y** is called a task-related component (TRC). Equivalently, TRCA is formulated as a Rayleigh-Ritz eigenvalue problem as

$$\hat{\mathbf{w}} = \arg\max_{\mathbf{w}} \frac{\mathbf{w}^{\top}\mathbf{S}\mathbf{w}}{\mathbf{w}^{\top}\mathbf{Q}\mathbf{w}} \tag{6}$$

These are treated as a generalized eigendecomposition problem $\mathbf{S}\mathbf{w} = \lambda\mathbf{Q}\mathbf{w}$, so **w** may be obtained as eigenvectors of the matrix $\mathbf{Q}^{-1}\mathbf{S}$. Note that, for the principal eigenvalue λ and eigenvector **w**,

$\lambda = \mathbf{w}^\top \mathbf{S} \mathbf{w} = \frac{1}{K(K-1)\tau} \sum_{k \neq \ell}^{K} \mathbf{y}^{(k)} \mathbf{y}^{(\ell)\top}$, so the eigenvalues are a measure of trial-to-trial reproducibility.

Generalized eigenvectors as a solution of the problem (5) or (6) are non-orthogonal because $\mathbf{Q}^{-1}\mathbf{S}$ is not symmetric. This is an advantage over using only the $\mathbf{S}$ matrix (like principal component analysis), where eigenvectors are constrained to be orthogonal to each other (Cohen, 2017, 2018). Once the filters are determined, corresponding spatial maps are constructed as detailed in (Haufe et al., 2014). If all of *N* eigenvectors are computed, *N* spatial maps corresponding to the eigenvectors are the columns of $\mathbf{W}^{-\top}$ where $\mathbf{W} = \begin{pmatrix} \mathbf{w}_1 & \cdots & \mathbf{w}_N \end{pmatrix} \in \mathbb{R}^{n \times n}$ is the eigenvector matrix. Here, we are interested in only a principal eigenvector **w**; in this case, the map is computed as $\frac{1}{T}\mathbf{X}\mathbf{y}^\top = \frac{1}{T}\mathbf{X}\mathbf{X}^\top \mathbf{w} = \mathbf{Q}\mathbf{w}$.

Note that if we introduce $\mathbf{v} = \mathbf{Q}^{1/2}\mathbf{w}$ and $\tilde{\mathbf{S}} = \mathbf{Q}^{-1/2}\mathbf{S}\mathbf{Q}^{-1/2}$, the optimization problem becomes

$$\text{maximize } \mathbf{v}^\top \tilde{\mathbf{S}} \mathbf{v} \text{ subject to } \mathbf{v}^\top \mathbf{v} = 1, \tag{7}$$

where $\mathbf{Q}^{1/2}$ is a symmetric matrix root of **Q**, hence $\tilde{\mathbf{S}}$ is a symmetric matrix. This is equivalent to formulation of principal component analysis (PCA), so various methods developed for PCA such as sparse PCA (d'Aspremont et al., 2005; Zou et al., 2006) and incremental PCA (Artac et al., 2002; Weng et al., 2003) can be applied to TRCA, but we will not discusses them here.

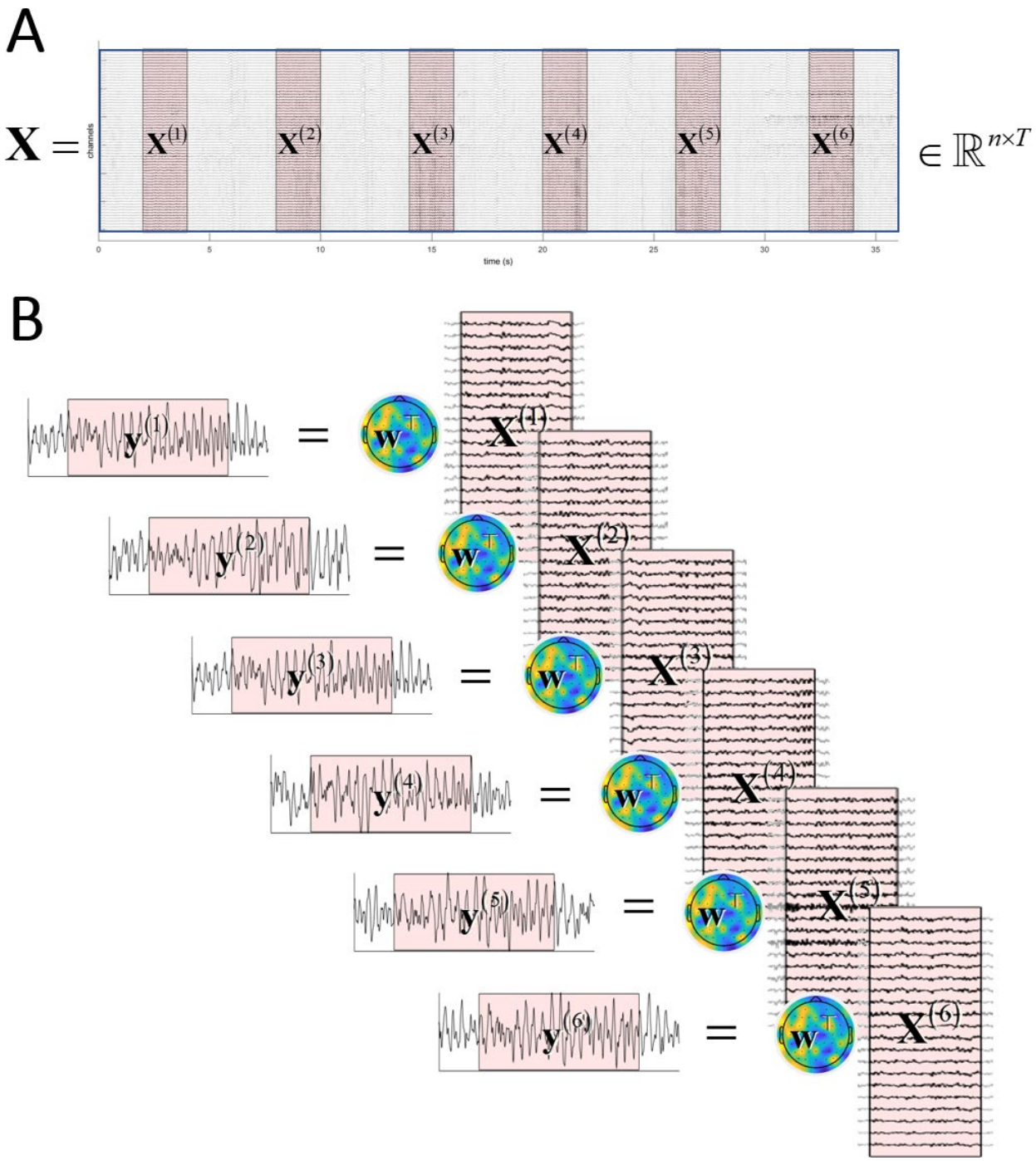

Figure 1. Schematic illustration of TRCA. (A) EEG data is given in terms of $n \times T$ matrix $\mathbf{X}$ and single-trial (i.e., event-relatedly time-windowed data) matrices $\mathbf{X}^{(k)}$ $\left(k = 1, \cdots, K\right)$. (B) The trial-reproducible components $y^{(k)}$ as weighted sums of single-trial matrices. The spatial filter **w** is determined so that *k*-th window activity $y^{(k)}$ and ℓ-th window activity $y^{(\ell)}$ are maximally correlated (i.e., reproducible).

2.2. Cross-correlation task-related component analysis (xTRCA)

Below we consider a problem of aligning temporal offsets of a TRC across trials as illustrated in Figure 2. Latencies of neural responses have intrinsic variability even with preferred stimuli. This raises a concern that TRCA may fail to discover a TRC if its latency jitters across trials i.e., if it does not phase-reset to event onsets. We address this problem by simultaneously optimizing both the spatial filter **w** and the timing vector **t**. It is formulated as a maximization problem of the Rayleigh-Ritz quotient with respect to the spatial filter **w** and the timing vector **t** as

$$\max_{\mathbf{w},\mathbf{t}} \frac{\mathbf{w}^\top \mathbf{S}(\mathbf{t})\mathbf{w}}{\mathbf{w}^\top \mathbf{Q}\mathbf{w}}. \tag{8}$$

In the original formulation of TRCA, the timing vector $\mathbf{t} = (t_1, \cdots, t_K)^\top \in \mathbb{R}^K$ is experimentally defined as event onset latencies. Components of the timing vector are referred to trial timings hereafter. Here, we introduce a new assumption; **t** varies from trial to trial because it represents hidden jitters of TRC, and it is no longer the same as the experimental event onset latencies. The proposed algorithm xTRCA achieves maximization of trial-reproducibility through iterative optimization of a spatial weight vector and a timing vector alternatively,

$$\max_{\mathbf{t}} \max_{\mathbf{w}} \frac{\mathbf{w}^\top \mathbf{S}(\mathbf{t})\mathbf{w}}{\mathbf{w}^\top \mathbf{Q}\mathbf{w}}. \tag{9}$$

The timing vector should be optimized to the direction of maximizing the eigenvalue, which is a measure of reproducibility hence serves as the objective function for this cross-correlation solution as well. When

a spatial filter of TRCA **w** is obtained with a timing vector **t**, one element of the timing vector is updated. A trial timing of the analysis window at *k*-th trial (t_k) is adjusted in order to maximize the eigenvalue. As *k*-th component of the timing vector is updated as $t_k \to t_k'$ while the other trial timings remain unchanged, the time-windowed data of *k*-th trial is updated as $\mathbf{X}^{(k)} \to \mathbf{X}^{(k)\prime}$. The matrix **S** is updated accordingly as

$$\begin{aligned}\Delta\mathbf{S}\left(t_k'\right) &= \mathbf{S}\left(\left\{t_1,\cdots,t_k',\cdots,t_K\right\}\right)-\mathbf{S}\left(\left\{t_1,\cdots,t_k,\cdots,t_K\right\}\right)\\ &= \sum_{\ell(\neq k)}\left\{\left(\mathbf{X}^{(k)\prime}-\mathbf{X}^{(k)}\right)\mathbf{X}^{(\ell)\top}+\mathbf{X}^{(\ell)}\left(\mathbf{X}^{(k)\prime}-\mathbf{X}^{(k)}\right)^{\top}\right\}.\end{aligned} \tag{10}$$

This change in the matrix **S** results in the change of eigenvalues. Here we use a technique from matrix perturbations because $\Delta\mathbf{S}$ is small compared with **S** because only one trial changes its value at a time. It is known that, to the first-order approximation, the eigenvalue is updated as

$$\Delta\lambda\left(t_k'\right) = \mathbf{w}^{\top}\Delta\mathbf{S}\left(t_k'\right)\mathbf{w}, \tag{11}$$

where **w** is the eigenvector of the original matrix **S**. This formula provides a guidance for how to update the timing vector. Using the definition of TRC and Eq. (10), the change in the eigenvalue (11) becomes

$$\Delta\lambda\left(t_k'\right) = 2\left(K-1\right)\left\{\mathbf{y}^{(k)\prime}\overline{\mathbf{y}}^{(k)\top}-\mathbf{y}^{(k)}\overline{\mathbf{y}}^{(k)\top}\right\}. \tag{12}$$

Here, $\overline{\mathbf{y}}^{(k)} \equiv \frac{1}{K-1}\sum_{\ell(\neq k)}^{K}\mathbf{y}^{(\ell)}$ is the trial average of TRCs except *k*-th trial. The second term is independent of t_k', so maximizing the eigenvalue equals to maximizing the cross-correlation between $\mathbf{y}^{(k)\prime}$ and $\overline{\mathbf{y}}^{(k)}$. In other words, the TRC time window of *k*-th trial should have maximal overlap with those of other trials. The new window latency should increase the perturbed eigenvalue, which is the objective measure of

reproducibility. We derive an update formula as

$$t_k \leftarrow \underset{t_k' \in [t_k - t_{\text{search}}, t_k + t_{\text{search}}]}{\arg\max} \mathbf{y}^{(k)\prime} \overline{\mathbf{y}}^{(k)\top} . \tag{13}$$

Therefore, the timing of *k*-th trial is optimized by maximizing the cross-correlation. The search area is restricted to $[t_k - t_{\text{search}}, t_k + t_{\text{search}}]$ so that the updated TRC time window stays around the behavioral event onset. We note that Eq. (13) is regarded as Woody's formula where $\mathbf{y}^{(k)\prime}$ is cross-correlated with a template $\overline{\mathbf{y}}^{(k)}$, so we derive Woody's formula using the same objective function, i.e., the eigenvalue. The above formula is valid when the matrix perturbation $\Delta\mathbf{S}$ is sufficiently small compared with **S**, so the timing optimization must involve a single trial at a time and the process needs to be iterated. Note that xTRCA does not determine an absolute latency of TRC if a window of analysis is longer than an actual TRC. This means that eigenvalues are invariant under translation of all time windows, namely $t_k \to t_k + a$ where *a* is a constant. Our algorithm resolves this uncertainty by requiring the trial average of time shift is zero.

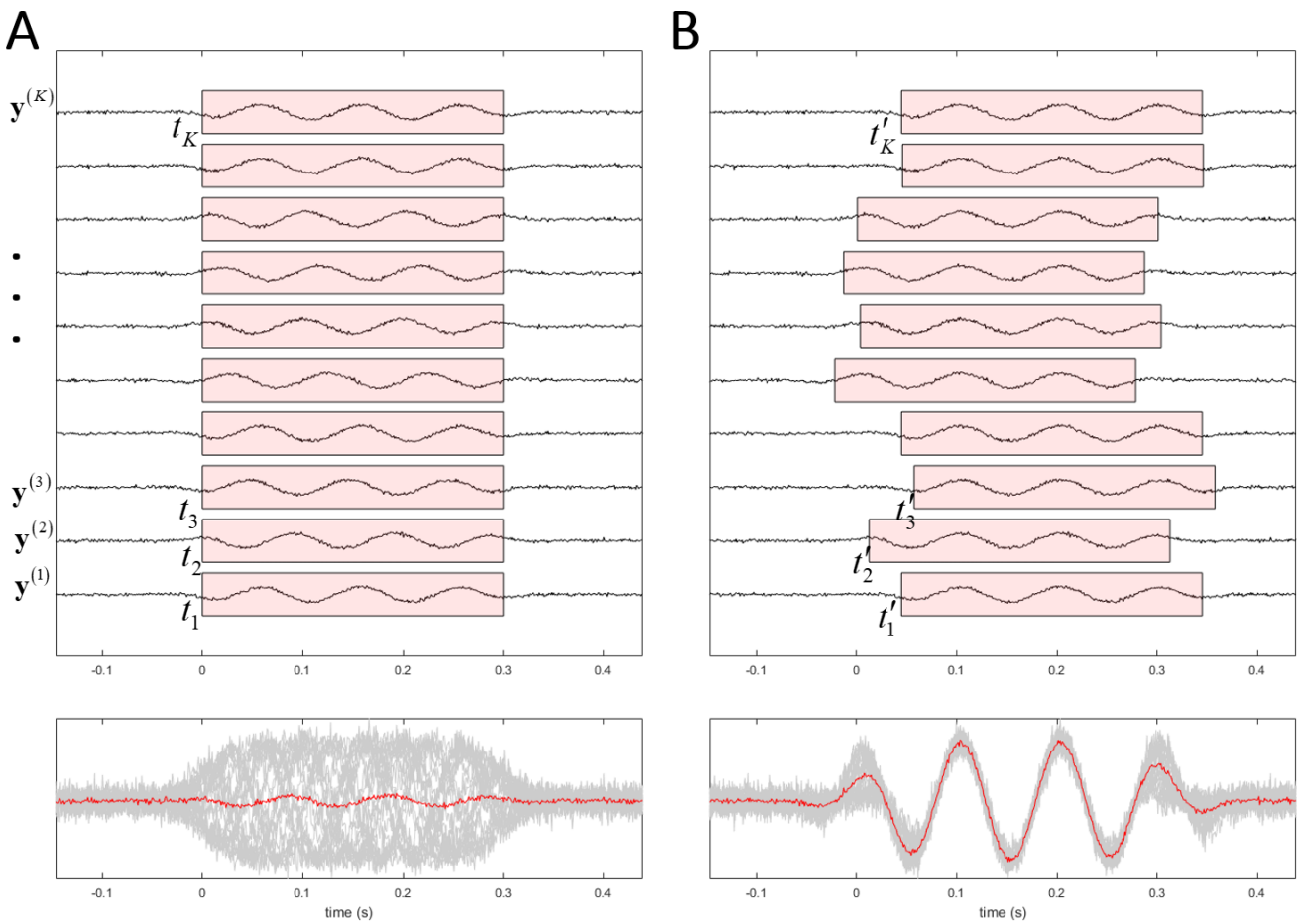

Figure 2. Schematic illustration of the cross-correlation method which is an extension from the conventional trial-reproducible component analysis (TRCA). (Left) Induced responses are by definition non-phase locked to an event onset at latency zero, which cancel out in averaging and result in a flat ERP waveform. (Right) The same induced responses whose phase/latency offsets are aligned to maximize trial reproducibility so that averaging the trials produces pronounced ERP waveform.

2.3. xTRCA algorithm

Here we summarize the xTRCA algorithm. Let us suppose the initial timing vector $\mathbf{t}_0 = (t_1, \cdots, t_K)^\top$ is provided as experimental event onset latencies that define the centers of the search areas. The algorithm

requires two parameters: a length of time window (τ) for constructing a spatial filter, and a search range (t_{search}) for optimizing trial timings. The search range is defined to be symmetrical relative to the current timing t, so the range is $\left[t_k - t_{\text{search}}, t_k + t_{\text{search}}\right]$ with the search parameter t_{search}.

The algorithm iteratively optimizes a spatial filter $\mathbf{w}$ with a given timing vector and updates the timing vector $\mathbf{t}$ with the optimized spatial filter. Both update steps of the spatial filter and the timing vector guarantee that eigenvalue is non-decreasing over iterations. In this process, how to select a trial to update remains an open question. After empirical testing, we propose a cyclic sampling of trials so that there are no trials that are not updated. The algorithm is summarized below:

Input: EEG data $\mathbf{X} \in \mathbb{R}^{n \times T}$, initial timing vector $\mathbf{t}_0$, a length of time window τ, search range t_{search} and a convergence threshold ε.

1. Initialize $\mathbf{t} \leftarrow \mathbf{t}_0$ as a timing vector.
2. Set λ_{old} as the dominant eigenvalue of TRCA with the given timing vector $\mathbf{t}$.
3. For trial k from 1 to K, iterate step 3.1 and 3.2.

   3.1. With a current timing vector $\mathbf{t}$, update weight by computing the principal eigenvector associated with the largest eigenvalue by solving

$$\mathbf{w} \leftarrow \arg\max_{\mathbf{w}} \frac{\mathbf{w}^{\top}\mathbf{S}(\mathbf{t})\mathbf{w}}{\mathbf{w}^{\top}\mathbf{Q}\mathbf{w}}. \tag{14}$$

   3.2. With a current spatial filter $\mathbf{w}$, slide a TRC window of k-th trial as

$$t_k \leftarrow \arg\max_{t'} \mathbf{w}^\top \Delta\mathbf{S}\left(t_k'\right)\mathbf{w} = \arg\max_{t'} \mathbf{y}^{(k)\prime}\overline{\mathbf{y}}^{(k)\top}. \tag{15}$$

4. Compute the dominant eigenvalue λ with the current timing vector $\mathbf{t}$.

5. Iterate Steps 2-4 until the dominant eigenvalue converges within a specified threshold as

$$\frac{\left\|\lambda_{\text{old}} - \lambda\right\|}{\left\|\lambda\right\|} < \varepsilon. \tag{16}$$

6. Compute the mean of temporal shift $\mathbf{t} - \mathbf{t}_0$ and subtract it from $\mathbf{t}$.

Output: Spatial filter **w**, and optimized timing vector **t**.

This algorithm ensures that timings of all trials are adjusted in Step 3. For our data sets, a solution was converged usually within four to five cycles of iterations with our choice of convergence criterion $\varepsilon = 10^{-4}$. We remark that, although a global maximum is not guaranteed, the eigenvalue is non-decreasing in Steps 3.1 and 3.2, so the algorithm achieves at least a local maximum. The optimized timing vector $\mathbf{t}$ is used for computing the **S** matrix and trial windows of xTRCA results. Matlab codes of the algorithm and analysis of synthetic data are attached as Supplementary Materials.

When more than one component are expected, the algorithm is iterated to extract a component one by one, a procedure known as deflation (Sameni et al., 2010). Suppose that one TRC, $\mathbf{y} = \mathbf{w}^\top\mathbf{X}$, is already obtained. Then, this TRC is projected out from the data matrix $\mathbf{X}$ by $\mathbf{X}\left(\mathbf{I} - \frac{\mathbf{y}^\top\mathbf{y}}{\mathbf{y}\mathbf{y}^\top}\right)$. Hence, by replacing the matrix $\mathbf{X}$ as $\mathbf{X} \leftarrow \mathbf{X}\left(\mathbf{I} - \frac{\mathbf{y}^\top\mathbf{y}}{\mathbf{y}\mathbf{y}^\top}\right)$ and applying the algorithm, a second component may be estimated. This deflation procedure can be iterated to obtain multiple components.

2.4. Statistical test for trial reproducibility

Since our proposed method optimizes both in the spatial and time domains, there is a risk of overfitting to data, potentially leading to a spurious component that seemingly resembles some ERP component even when there are in fact no reproducible components in the data. Therefore, a statistical test is needed to assess whether the component extracted by the algorithm is statistically reproducible or merely an artifact due to overfitting to data. Since the eigenvalue is a measure of reproducibility, we here propose a resampling-based statistical test of eigenvalue (Tanaka et al., 2013). The underlying assumption of xTRCA is that there are reproducible signals mildly time-locked to trial onsets with variable onset jitters. Accordingly, we posit a null hypothesis that there are no reproducible signals time-locked to trial onsets. If the null hypothesis holds, the value of eigenvalue that is computed based on trial timings is statistically indistinguishable from those computed based on randomized timings. Therefore, a null distribution of eigenvalues is computed by sampling a randomized timing of k-th trial $\left(k = 1.\cdots, K\right)$ from a uniform distribution,

$$t_k \sim U\left(t_{\text{search}}, T - \tau - t_{\text{search}}\right) \tag{17}$$

where T is the length of EEG data, τ is the length of time window, and t_{search} is the length of search window. Statistical significance of the eigenvalue based on trial timings is evaluated against the null distribution. For the synthetic and real data described below, we iterated the resampling procedures 1,000 times to compute the null distributions.

2.5. Analysis of synthetic induced response

Simulated scalp EEG data of 64 channels were generated using 2004 cortical dipole sources and a forward model implemented in OpenMEEG software (Tadel et al., 2011; Cohen, 2017). The duration of the data was 85 seconds, and there were 80 trials (K =80) separated by one second. To simulate an induced response of k-th trial, we defined the following signal as the ground truth of TRC in this simulation.

$$\frac{1}{1+e^{-(t-t_k)/a}} \cdot \frac{1}{1+e^{t-t_k-\tau/a}} \cdot \cos\left(2\pi f\left(t-t_k\right)+\theta_k\right). \tag{18}$$

Here, the two sigmoid functions determine a response envelope of size τ, and the cosine term determines an oscillatory response within the envelope. Here the frequency f and the window size τ was 10 Hz and was 300 ms, respectively, so the time window contained three cycles of EEG alpha band (8-13 Hz). The rise parameter a was 15 ms. The phases $\{\theta_k\}_{k=1}^{K}$ were taken from eight values ($-7\pi/8, -5\pi/8, -3\pi/8, -\pi/8, \pi/8, 3\pi/8, 5\pi/8, 7\pi/8$). There were 10 trials for each phase value, total of 80 trials. The trial onset latencies were 1, 2, 3, …, 80 seconds, thus the initial timing vector was $\mathbf{t}_0 = (1, 2, \cdots, 80)^\top$. We used the synthetic time series for one dipole in the occipital lobe, MNI [5 -82 24], and bandpass filtered Gaussian noises for the other 2003 dipoles. The time series of dipole source activities were projected onto the 64 channels on the scalp using the lead-field matrix computed by OpenMEEG.

xTRCA was applied to the simulated data set with a TRC window length of 450 ms and the search-window length of 60 ms to search the hidden onset of TRC within a window of [-60 ms , + 60 ms] relative to the initial timings. The iterative process was repeated until the convergence criterion was met, resulting

in an optimal spatial filter and timing vector. The spatial filter was converted into a scalp topography and compared with that projected from the ground-truth occipital dipole; the timing vector was converted into phase shifts by multiplying $2\pi f$ and compared with the phases $\{\theta_k\}$ that were specified in the synthetic data. The mean value of the timing vector was subtracted. The statistical significance of the eigenvalue was evaluated by the resampling-based test. For a comparison, the original TRCA (i.e., the spatial filter only) was applied to the same synthetic data. We also looked at single-channel data at channel Oz. To evaluate the effect of timing optimization, Woody's method was applied to the single-channel data, referred to as cross-correlation Oz or xOz.

Additionally, to compare the scalp topographies computed by xTRCA and TRCA, the above simulation was repeated for 100 times by varying ground-truth source dipole locations. The location was randomly chosen from 2004 dipoles for every iteration while other conditions kept equal, and the scalp topographies were computed by xTRCA and TRCA. Accuracy of these maps was quantified by computing correlation coefficients between the original and the recovered scalp topographies.

Finally, to examine if xTRCA could extract multiple TRCs, two sources were simulated using Eq. (18); one in the occipital lobe (MNI [5 -82 24]) with $f = 10$ (Hz), $a = 15$ (ms), and $\tau = 200$ (ms), and another in the parietal lobe (MNI [-42 -48 70]) with $f = 20$ (Hz), $a = 7.5$ (ms), and $\tau = 200$ (ms). These sources were spatially separated in the cortex, but their scalp topographies had partial overlaps due to volume conduction, and their activities were temporally overlapped. The phases of the two sources were independently trial-by-trial randomized as in the single-source simulations. Simulated scalp EEG

data were created using the same lead-matrix described above. We the applied the xTRCA iteratively to examine if the two TRCs were recovered. The same window length ($\tau = 450$ ms) and the search range [-60 ms , + 60 ms] were used for the analysis of synthetic two-source data.

2.6. Analysis of mismatch negativity data

To validate xTRCA in enhancing event-related responses in real-data application, we analyzed EEG data recorded from three healthy adult subjects during a classical duration mismatch negativity (MMN) task. The details of the experiment and analyses can be found in (Rissling et al., 2012). Briefly, 40-channel EEG data were recorded during a passive auditory duration mismatch negativity task; two kinds of auditory stimuli, frequent standard (1 kHz tone with 50-ms duration) and rare duration-deviant (1 kHz tone with 100-ms duration) were presented as non-attended background auditory stimuli while a subject watched a silent movie throughout the recording. The inter-stimulus interval was 500 ms. The three subjects received 2168, 2119, and 2778 standard stimuli, and 317, 257, and 337 deviant stimuli, respectively. Before applying xTRCA, the data was preprocessed as follows using EEGLAB and its plugins (Delorme and Makeig, 2004). The sampling rate of original data was 1000 Hz and down-sampled to 250 Hz to save the computational time and storage memory. The data was first high-pass filtered using a basic FIR filter (cutoff frequency 0.5 Hz, transition bandwidth 1 Hz, Hamming windowed). Line noise at 60 Hz and its second harmonics at 120 Hz were then removed by the CleanLine EEGLAB plug-in which adaptively estimates and removes sinusoidal artifacts using a frequency-domain regression technique

(Mitra, 2007). Finally, non-stationary high-amplitude artifacts such as eye blinks, muscle, and electrode motion were removed by applying the artifact subspace reconstruction (ASR) method, which is implemented as the clean_rawdata plugin (Mullen et al., 2015). Variances of EEG data processed by ASR became relatively constant, so the assumption of stationarity was assured (Tanaka et al., 2018). The inputs to the algorithm were the preprocessed, continuous EEG data (denoted by $\mathbf{X}$) and the experimental stimulus onsets (denoted by $\mathbf{t}_0$).

xTRCA was applied to the two conditions separately to compute TRCs and the corresponding scalp topographies. To match the numbers of trials for a comparison, first 200 trials of the two conditions were analyzed. The length of the analysis window τ was set to 400 ms, and the search window [-120 ms, +120 ms] relative to sound stimulus onset latency. This window length (400 ms) was chosen so that it was long enough to cover conventional MMN waveforms and short enough to avoid adjacent trials separated by the inter-stimulus interval of 500 ms. Spatial filter $\mathbf{w}$ and timing vector $\mathbf{t}$ were optimized by the xTRCA algorithm. Statistical significance of the eigenvalues was evaluated by applying the resampling-based test. A statistical difference between TRCs of the two conditions obtained from xTRCA were assessed by performing a nonparametric permutation test corrected by the Benjamini-Hochberg procedure (Benjamini and Hochberg, 1995). Finally, for a comparison, single-channel data at Fz, where mismatch negativity responses are conventionally defined, was analyzed, and TRCA with the stimulus onsets $\mathbf{t}_0$ was applied.

2.7. Classification analysis

For a practical application such as brain-computer interfaces, a detection of reliable ERP waveforms plays a key role in achieving successful performance (Mak et al., 2011). A typical brain-computer interface consists of two analysis steps, first to extract features from data, and then to classify trials based on the extracted features. Features must be reproducible across trials of a same condition, so our method can improve the performance of feature extraction step. Most methods to enhance ERPs for brain-computer interfaces rely on spatial filtering of multiple channels (Blankertz et al., 2008), but curiously a possible application of temporal optimization has not been largely pursued, with a few notable exceptions (Thompson et al., 2013; Arico et al., 2014; Mowla et al., 2017). Therefore, to illustrate a possible application of our proposed method, we performed an analysis to classify single-trial TRCs of standard and deviant trials using the same data analyzed above. Data from standard and deviant trials were subjected to one type of classifiers, sparse linear discriminant analysis (sLDA) (Clemmensen et al., 2011). sLDA automatically select a small number of features relevant to a classification, so there is no need to select features or to decimate by hand, such as temporal averaging. Single-trial waveforms both for standard and deviant conditions were extracted either from the single channel (Fz), TRCA or xTRCA. These waveforms were subjected to an sLDA classification analysis. We used a Matlab implementation of sLDA, the spaSM toolbox (Sjöstrand et al., 2018). Performance of classification was evaluated by randomly choosing 10% of the data for training a classifier and then applying the classifier to the rest of the data (i.e., 10-fold cross validation). The classification error was computed as a measure of classification performance.

3. Results

3.1. Synthetic data

Our prediction was that xTRCA should recover the ground-truth TRC and scalp topography by simultaneously optimizing the spatial filter and trial timings (see Section 2.4). Before applying xTRCA, neither the simulated dipole source ERP or its noisy projection to a scalp channel Oz showed distinguishable ERP waveform (Figure 3A, B). First, we applied a single-channel cross-correlation to evaluate performance of optimizing the timing vector alone without using the TRCA spatial filter (xOz). Trial-timing optimization alone could recover the sinusoidal waves embedded in the synthetic data, albeit noisy (Figure 3C). We then observed that the conventional TRCA spatial filter failed to resolve the ground-truth of the jitter in TRC even though the spatial filter roughly detected the source projection (Figure 3D). In contrast, xTRCA successfully resolved both the TRC waveform and the scalp topography (Figure 3E). Finally, xTRCA correctly found the eight clusters of relative phases, which was the ground truth of the phase distribution (Figure 3F). Cross-correlation coefficients between all possible trial pairs were computed to quantify trial reproducibility of the four methods (Oz, xOx, TRCA and xTRCA). Mean values of cross-correlation coefficients across trial pairs were -0.0032 (SD 0.20) for Oz (Figure 3B), 0.26 (SD 0.051) for xOz (Figure 3C), 0.010 (SD 0.058) for TRCA (Figure 3D), and 0.84 (SD 0.029) for xTRCA (Figure 3E), therefore xTRCA performed best in suppressing the trial-by-trial variability of ERPs. The spatial and temporal optimization of xTRCA functioned as expected in recovering the ERP waveform, the scalp topography, and the trial timings. Finally, the resampling-based test suggested that the eigenvalue

based on the trial timings was statistically significant against the null distribution ($p < 10^{-4}$), indicating that xTRCA correctly identified the reproducible signals without overfitting.

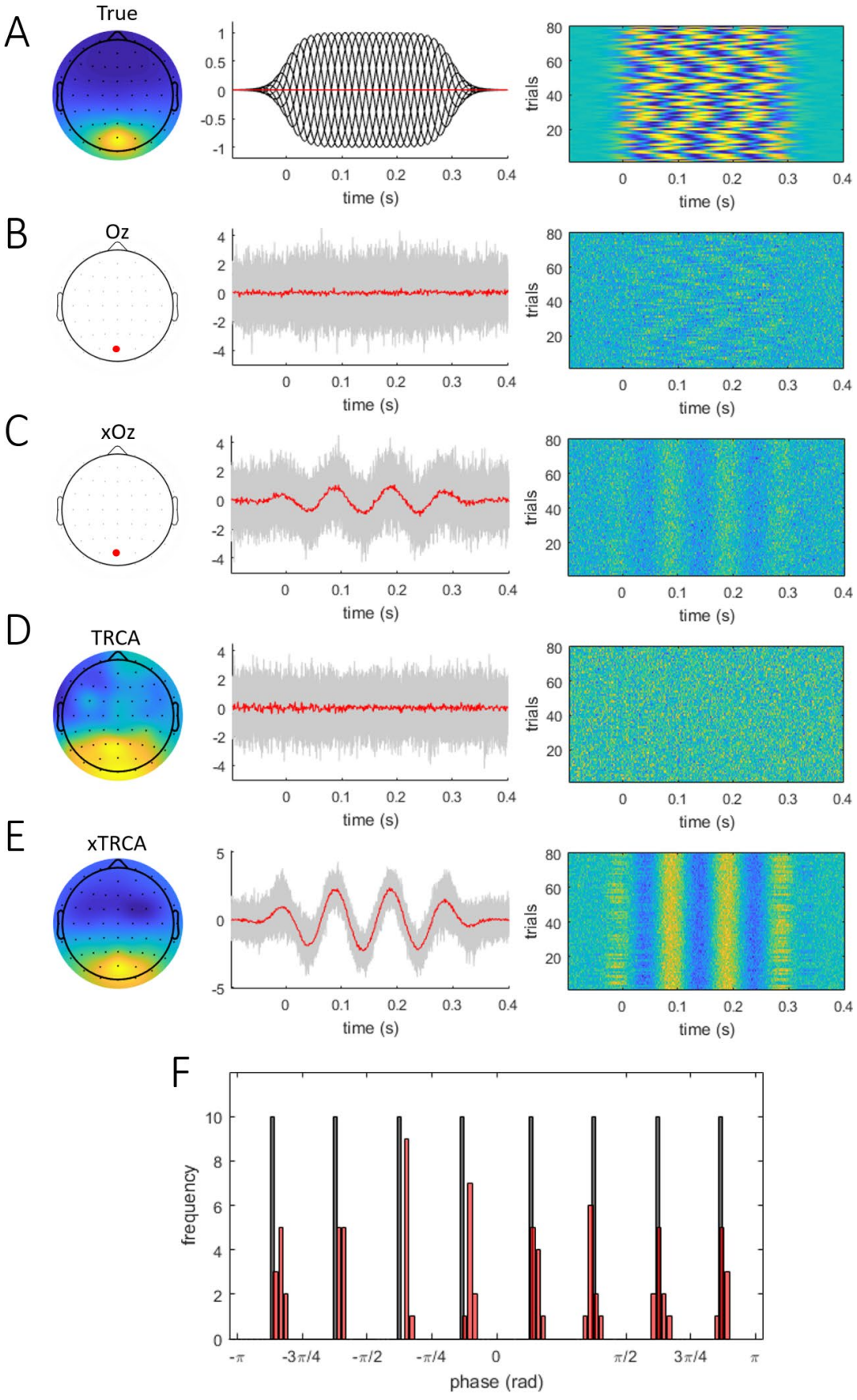
A
True
B
Oz
C
xOz
D
TRCA
E
xTRCA
F
time (s)
trials
frequency
phase (rad)
-π
-3π/4
-π/2
-π/4
0
π/2
3π/4
π

Figure 3. Results from the simulated data analysis. (A) Ground-truth trial-reproducible component (TRC) which is simulated induced responses. A short-burst of 10-Hz sine waves of 80 trials with 10 equidistantly distributed phases. The source dipole was localized at [5 -82 24] within the MNI template head. (B) A trial-averaged ERP waveform and a trial-concatenated ERP image of scalp EEG at electrode Oz aligned to external event onsets. (C) The results after optimizing trial timings of single-channel data at Oz by cross-correlation (xOz). (D) Results from TRCA and (E) xTRCA. (F) Histograms showing phases of the ground-truth signals (black) and the xTRCA recovered signals (red). The recovered phases were computed from the difference between response and event timings multiplied by $2\pi f$, where f was the frequency of induced activity (10 Hz) (See Eq. (18)).

Above, we observed that the scalp topographies found with and without temporal optimization differed. To systematically evaluate the difference in recovered scalp topographies between TRCA and xTRCA, the same simulation was repeated 100 times while varying the source dipole location. Examples of the results are illustrated in Figure 4A. As shown in Figure 4B, the scalp topographies obtained by xTRCA showed far better correlation to the ground-truth scalp topographies than those obtained by TRCA; means of correlation coefficients, 0.97 (SD 0.008) for xTRCA and 0.65 (SD 0.28) for TRCA, respectively. This result suggests that scalp topographies identified by a spatial filter alone could lead to incorrect and misleading estimation and that optimization of trial timings along with a spatial filter improved the reliability of scalp topographies.

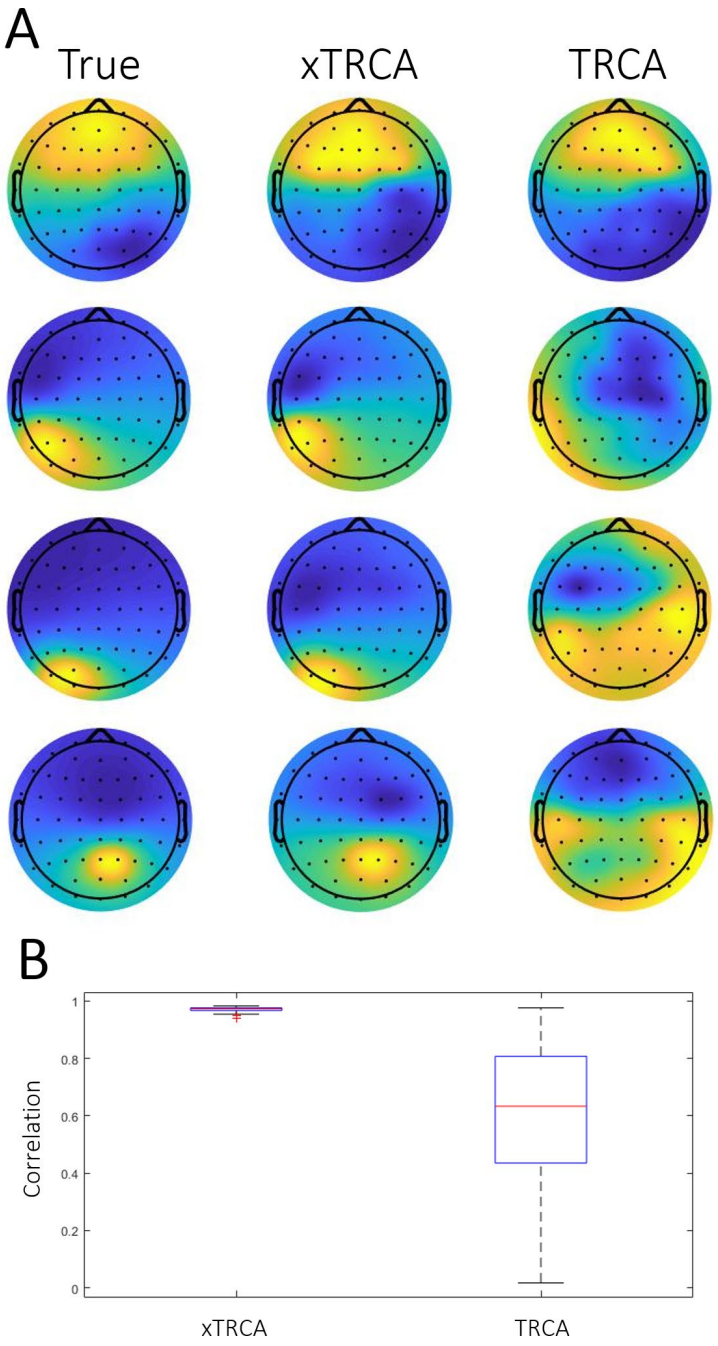

Figure 4. Scalp topographies recovered by the TRCA and xTRCA. (A) Four representative examples of the ground-truth scalp topographies projected by simulated source dipoles (left column), those recovered by xTRCA (middle column), and those recovered by TRCA (right column). (B) A box plot of correlation coefficients between the ground-truth scalp topographies and those produced by xTRCA (left), and the same by TRCA (right).

Finally, we tested whether the xTRCA algorithm could recover multiple TRCs using a deflation method. Two sources of induced activities, one in the occipital lobe and another in the parietal lobe, were simulated to generate synthetic scalp EEG data, and the xTRCA algorithm was applied. We observed that the two TRCs were successfully recovered with the correct scalp topographies and onset-aligned waveforms in the ERP images (Figure 5). The phases were also correctly recovered. Despite that the activities of the two sources were overlapped in time and partially in scalp topographies, the algorithm could rightly recover the scalp topographies, the wave forms, and the trial onsets (or the phases).

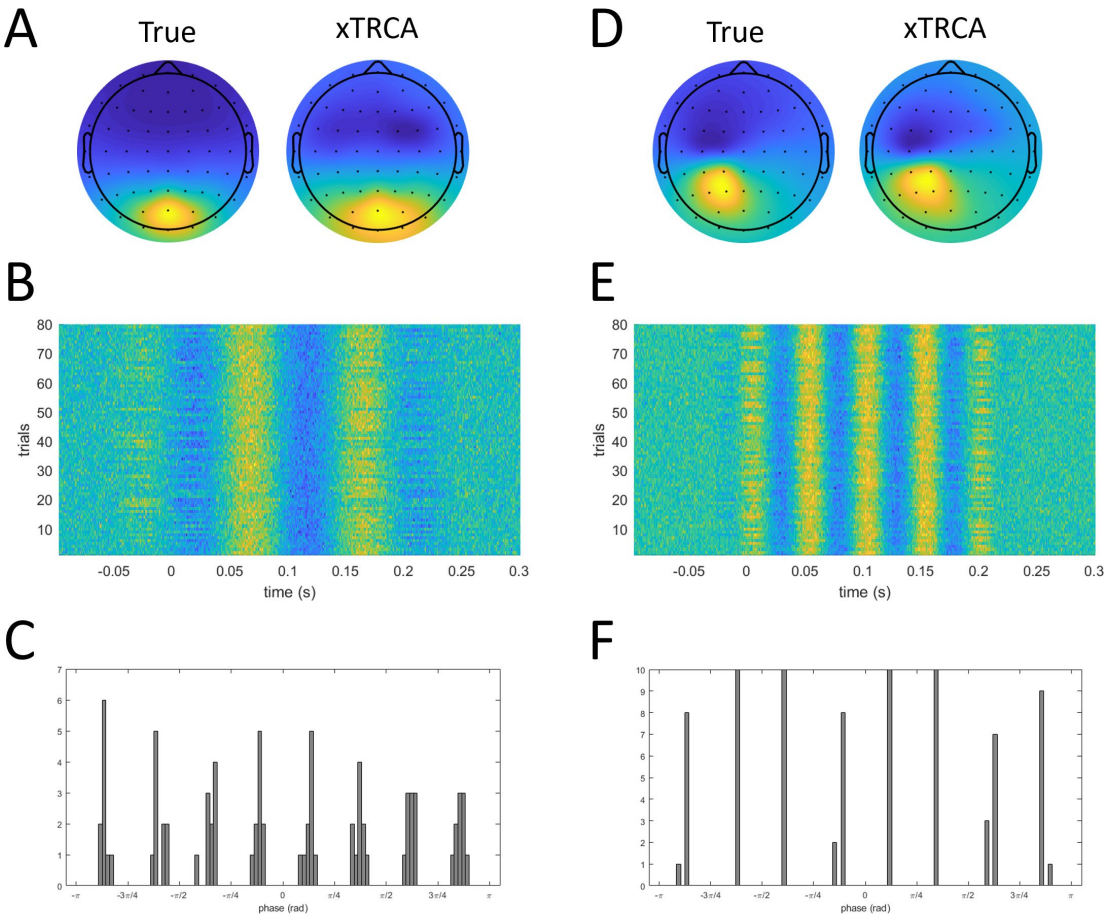

Figure 5. Results of analysis of two-source synthetic data. (A) Comparison of scalp topographies, (B) ERP image, and (C) a histogram of the optimized trial onsets are shown for the component 1 located at the occipital lobe. (D-F) for the

component 2 located in the parietal lobe.

3.2. Mismatch Negativity Data

We further tested whether and how the xTRCA algorithm improved ERPs in the mismatch negativity experiment. The xTRCA algorithm was applied to the trials of frequent standard stimulus and those of rare duration-deviant stimulus separately. For comparison, the same data were analyzed at the single channel (Fz) and TRCA. The results of three representative subjects are summarized in Figures 6, 7 and 8, respectively. Typical waveforms for standard and deviant stimuli were observed at the channel Fz (Figures 6A, 7A, and 8A), and those waveforms were considerably enhanced both by TRCA (Figures 6B, 7B, and 8B) and xTRCA (Figures 6C, 7C, and 8C). ERP images of standard condition (Figures 6D-F, 7D-F, and 8D-F) and of deviant condition (Figures 6G-I, 7 G-I, and 8 G-I) confirmed that latency jitter in ERPs were well compensated by xTRCA. To quantify trial reproducibility of the three methods, cross-correlation coefficients between all possible trial pairs were computed with in the period from 100 ms to 400 ms (Table 1). The average cross-correlation coefficients using Fz, TRCA, xTRCA were 0.012 (SD 0.25), 0.070 (SD 0.24), 0.19 (0.22), respectively, for the standard condition, and 0.14 (SD 0.27), 0.39 (SD 0.27), 0.52 (SD 0.20), respectively, for the deviant condition. We therefore observed that xTRCA appreciably improved the reproducibility of ERPs across trials. Regarding scalp topographies, five of six scalp topographies were located in the frontal lobe including the channel Fz, while one (standard condition of subject 1) was found in the temporal lobe (Figures 6JK, 7JK, and 8JK). Finally, the distributions of

time shifts had a peak at the origin, and time shifts of deviant condition (Figures 6L, 7L, and 8L) were narrowly distributed than those of standard condition (Figures 6M, 7M, and 8M). Mostly for the standard condition, there were some trials whose time shifts were either on the lower or upper bounds, especially in the case of Subject #3 (Figure 8L), indicating that ERPs of standard condition were not tightly time-locked to the stimulus onsets. The resampling-based statistical test indicated that the eigenvalues for the deviant condition were statistically significant ($p < 10^{-4}$ for all the subjects), indicating that there were reproducible components time-locked to the trial onsets for the deviant condition. On the other hand, the eigenvalues for the standard condition were statistically non-significant ($p = 0.547$ for Subject #1, $p = 0.587$ for Subject #2, and $p = 0.041$ for Subject #3, Bonferroni corrected), indicating that the ERPs were not reproducible enough for the standard condition. In summary, xTRCA outperformed other methods by benefitting from optimizing both the spatial filter and the timing vector.

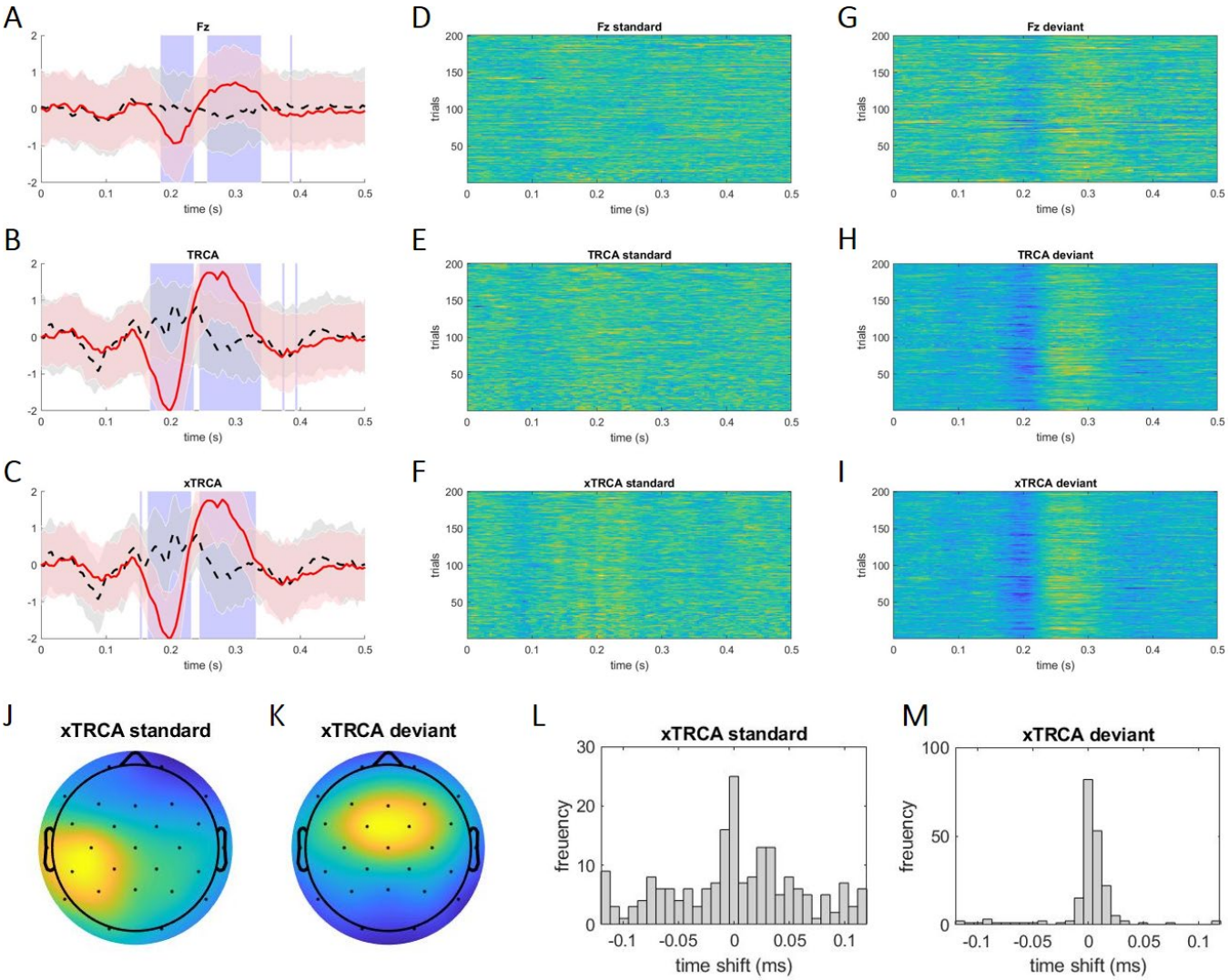

Figure 6. Results from the analysis of the mismatch-negativity data for Subject #1. (A) ERPs at channel Fz. The black broken line and red solid line depict ERPs of the standard and deviant conditions, respectively, accompanied by the shaded areas of the same colors representing the standard deviation. Blue shaded areas in the background indicate the periods where statistically significant differences between the two conditions were found. ERP images of (B) standard and (C) deviant conditions. (D-F) ERPs and ERP images computed by TRCA. (G-I) ERPs and ERP images computed by xTRCA. (J, K) Scalp topographies and (L, M) histograms of time shift computed by xTRCA for the two conditions.

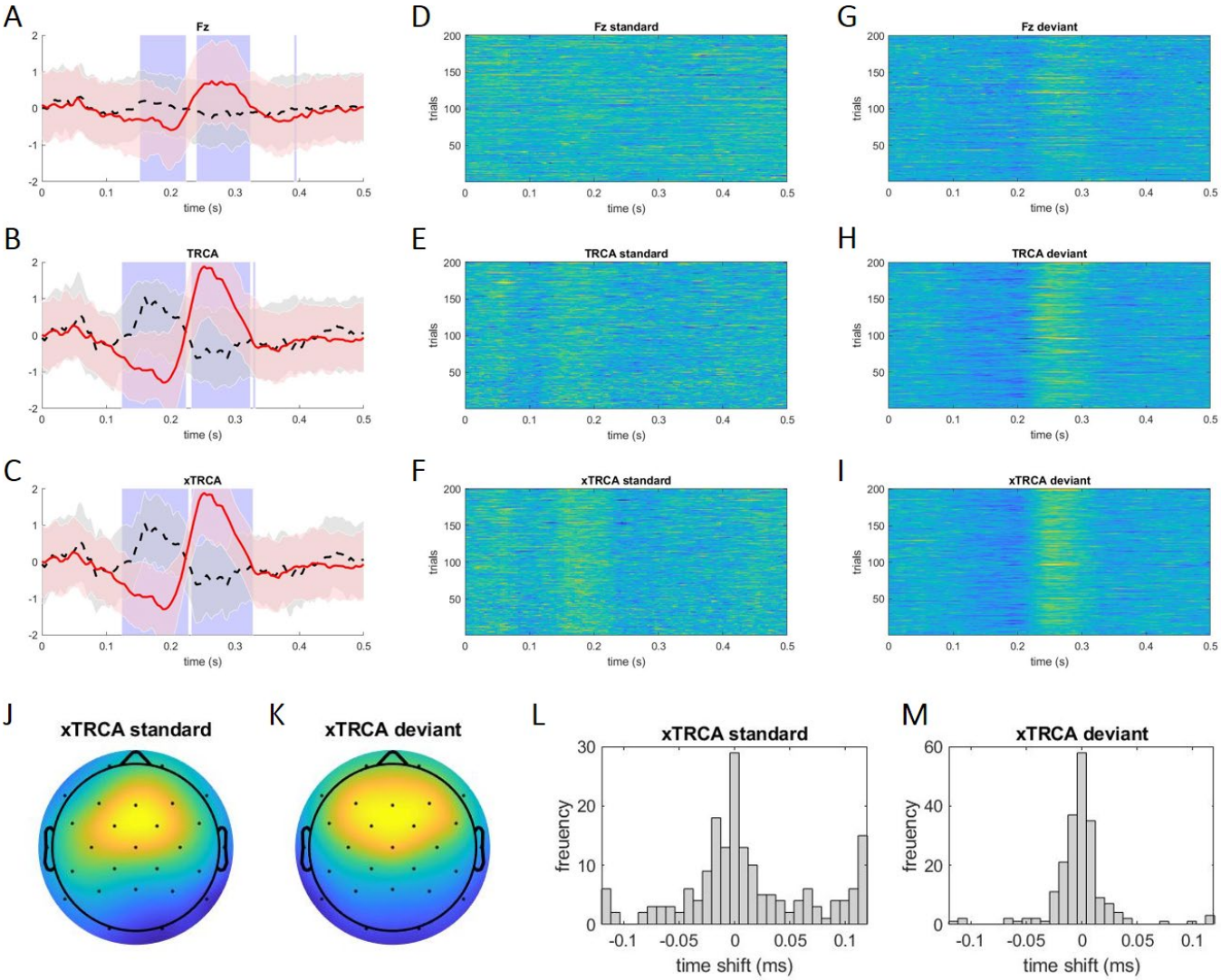

Figure 7. Results from the analysis of the mismatch-negativity data for Subject #2. The format is the same as Figure 6.

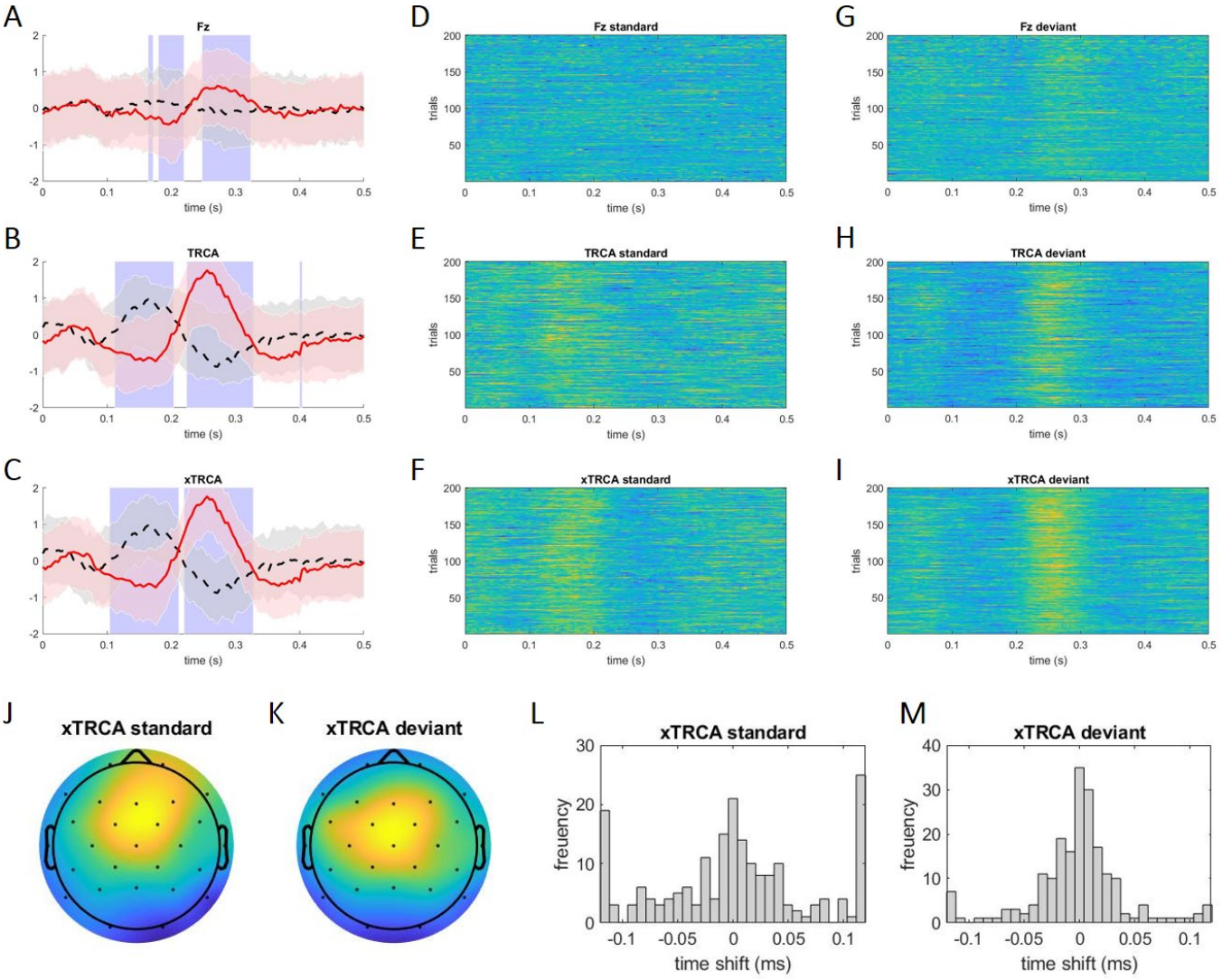

Figure 8. Results from the analysis of the mismatch-negativity data for Subject #3. The format is the same as Figure 6.

Table 1. Summary of cross-trial correlation coefficients. Mean values of correlation coefficients from all possible trial pairs were computed using single channel (Fz), TRCA and xTRCA. Numbers in the parenthesis represent standard deviations.

		Standard condition	Deviant condition
Fz	Subject #1	0.011 (0.24)	0.16 (0.27)
	Subject #2	0.015 (0.27)	0.14 (0.28)
	Subject #3	0.0088 (0.24)	0.086 (0.29)
TRCA	Subject #1	0.048 (0.20)	0.43 (0.26)
	Subject #2	0.074 (0.22)	0.42 (0.25)
	Subject #3	0.086 (0.29)	0.30 (0.29)
xTRCA	Subject #1	0.12 (0.19)	0.53 (0.19)
	Subject #2	0.20 (0.19)	0.53 (0.20)
	Subject #3	0.28 (0.23)	0.49 (0.22)

3.3. Classification analysis

We have demonstrated that xTRCA improved the reproducibility of ERPs between the two conditions. To suggest a possible application, we further performed a classification analysis between ERP waveforms from standard and deviant trials. Each time series from a single trial contained 76 sampling points, which spanned from 100 ms to 400 ms after the trial timing. Sparse LDA automatically assigned non-zero

weights to approximately 40% of the sampling points. Classification errors for the individual subjects were computed by 10-fold cross validation (Table 2). In summary, classification errors averaged over the three subjects were 0.25 (SD 0.070) for Fz, 0.11 (SD 0.57) for TRCA, and 0.030 (SD 0.040) for xTRCA, and the classification became considerably improved by xTRCA. Therefore, we demonstrated that xTRCA is a useful method for feature extraction step in brain-computer interfaces.

Table 2. Summary of classification error for the three methods.

		Classification error
Fz	Subject #1	0.23 (0.049)
	Subject #2	0.23 (0.066)
	Subject #3	0.28 (0.087)
TRCA	Subject #1	0.13 (0.055)
	Subject #2	0.070 (0.045)
	Subject #3	0.044 (0.14)
xTRCA	Subject #1	0.058 (0.049)
	Subject #2	0.020 (0.033)
	Subject #3	0.013 (0.013)

4. Discussion

The purpose of this study was to develop a time-domain analysis method that enhances ERPs in the time domain by optimizing both a spatial filter and trial timings, thereby expanding the conventional temporal averaging method both for evoked and induced responses. The proposed xTRCA achieved this goal by extending our previously published linear spatial filter method TRCA (Tanaka et al., 2013, 2014) with a cross-correlation method to estimate single-trial TRC latency jitters and to correct them using the common objective of trial reproducibility used in TRCA. It is a unified analysis method equally effective for both evoked and induced responses. The application of xTRCA to the mismatch negativity data from three subjects confirmed that the reproducibility of single-trial waveform was significantly improved and the classification error was considerably reduced. Further studies are warranted for investigating the natures of the novel/re-defined ERP peaks and troughs in relation to known ones. Particularly, it is critical to clarify whether the novel/re-defined ERP components show better or worse correlation to known behavioral measures. Once xTRCA is verified in these empirical testings in future studies, we expect that xTRCA will overcome a limit of conventional ERP studies with waveform analyses in the time-domain and will become a useful tool for cognitive neuroscience and brain computer interfaces.

4.1. Previous Approaches for enhancing ERPs

As briefly reviewed in Introduction, a number of studies reported increased inter-trial or inter-subject reproducibility of EEG responses by either spatial averaging or temporal recalibration. Using a method of spatial averaging, Huffmeijer and colleagues studied reproducibility of ERPs in response to

feedback stimuli of happy or disgusted faces across a four-week interval (Huffmeijer et al., 2014). They reported that spatial averaging over 7 or 17 electrodes increased intra-class correlations of P3 amplitudes, indicating that spatial averaging suppressed across-trial variability. Rather than simple spatial averaging, a few recent studies have proposed spatial filtering to maximize trial reproducibility of ERPs, including xDAWN, reliable component analysis, and TRCA. Whereas these approaches differ in technical details, they have a common goal of trial reproducibility. xDAWN formulates a forward model that describes how observed data is generated from reproducible components, and in contrast, reliable component analysis and TRCA formulate a backward model that describes how reproducible components are extracted from observed data. Also, xDAWN and TRCA assume trial reproducibility in the time domain, while reliable component analysis assumes trial reproducibility in the frequency domain.

On the other hand, there have been studies to enhance ERPs in single-channel data by canceling trial-by-trial variability of response onsets, starting the seminal work of Woody. Woody's method compensates trial-by-trial jitters by computing cross-correlation of a single-trial time course and a template and then shifting the time course by a peak location of the cross-correlation. There are recent extensions of Woody's method. Gips et al. (2017), for example, proposed a method for extracting recurrent wave forms by optimizing timings based on a Monte-Carlo search, specifically the Metropolis-Hastings method. They uncovered skewed (i.e., asymmetric) waves, instead of sinusoidal waves, of gamma oscillations in local field potentials from the rat hippocampus and monkey V1, and layer-specific skewed waves from the superficial and deep layers in the monkey V1. Whereas this approach adjusts latencies

without assuming any specific distributions of timings, the Monte-Carlo approach was essentially a random search and hence inefficient in terms of computational cost and time. Our method, in contrast, is designed to perform an explicit search for maximum eigenvalue, and the computational process is optimized to be fast for heavily iterative computation.

A few recent studies have developed a spatiotemporal approach much in line with our work. Most relevant to our work is spatio-temporal common pattern proposed by (Congedo et al., 2016). The method was a combination of the spatial filter (xDAWN) and temporal optimization (Woody's method) as in xTRCA, and was successfully applied to the analysis of evoked potentials of P3 data. Our study derives the spatial filter and temporal optimization using a single objective function (i.e., eigenvalue of the generalized eigenvalue problem) and extends to the analysis of induced potentials. Taken together, we believe that optimal integration of spatial filtering and temporal optimization provides a novel and powerful technique for analyzing and interpreting event-related potentials.

4.2. Consideration in Applying xTRCA Algorithm

The xTRCA algorithm contains the two parameters: the time-window size τ and the search range t_{search}. Through extensive numerical testing, we provide general recommendations on how the parameter values are determined. First, the time-window size should be determined based on the knowledge of ERPs and experimental conditions. For our case of the MMN experiment, the size of time window was determined so as to cover the known length of ERP responses and, at the same time, to avoid overlapping

with preceding or succeeding trials. Our value of 400 ms is long enough to include the MMN waveform and shorter than the inter-stimulus interval of 500 ms. Second, the search range should be set to a small range at the beginning and be increased gradually to avoid overfitting to background activities. The distribution of shifts of trial timings is bimodal when the search range is too small, the distribution becomes unimodal when the search range is sufficiently long.

The xTRCA has large degrees of freedom of adjusting the spatial filter and trial timings, so there is a risk of identifying a feature that is not directly relevant to an experiment in question. One possible feature is spontaneous, background activities. For some infrequent cases (a subject whose results were not included in the main text), we found that xTRCA extracted spontaneous, alpha-band components that were not necessarily phase-locked to experimental timing onsets (Figure 9A). This case was encountered in the analysis of standard condition where the ERP waveform did not have clear peaks and troughs. For this case, the scalp topography was located in the parieto-occipital lobe (Figure 9B), and the distribution of trial onsets was not peaked at the origin with no appreciable structure (Figure 9C), indicating that this component was not time-locked and resulted from a spontaneous alpha activity in the posterior area of the brain. Therefore, we regard this component as a task non-related, alpha-band component. xTRCA, therefore, must be used with care. For the analysis of MMN experiment data, we have compared the TRCs of xTRCA with the conventional ERPs from the single channel and confirmed that the characteristics of TRCs extracted by xTRCA were in line with those of single-channel ERPs. We recommend to examine

and confirm the results of xTRCA judiciously in consideration of the knowledge of ERPs characteristics in question.

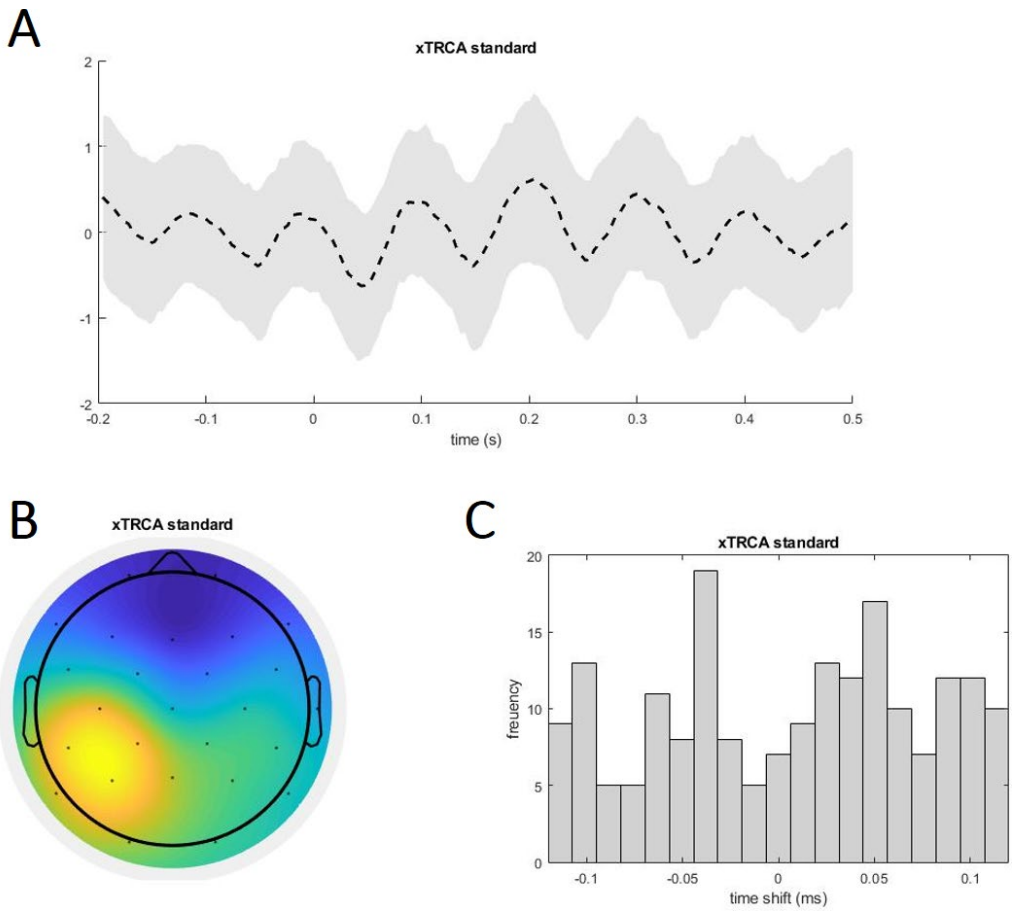

Figure 9. Example of an overfitting case where xTRCA incorrectly identified a spontaneous, background activity. (A) Trial-averaged waveform (black broken line), (B) scalp topography, and (C) histogram of time shifts.

As a solution to the issue of overfitting, we proposed the resampling-based statistical test based on the null hypothesis that there are no reproducible signals time-locked to trial timings. We observed that the eigenvalues were statistically significant for the synthetic data and for the deviant condition of the MNN data. We further validated the statistical test by simulating synthetic data with non-reproducible, random signals (instead of Eq. (18)) and found that the eigenvalue was not statistically significant against the null

distribution, as expected. In summary, the proposed test reported statistical significance when the data contained reproducible signals and statistical non-significance when the data contained non-reproducible signals, at least for the case of synthetic data. We therefore recommend to perform the resampling-based test to examine whether the component extracted by xTRCA is statistically reproducible or merely an artifact due to overfitting to data.

4.3. Problem of Latency Jitter in EEG analysis

It is long known that neural activities, measured either in single neurons or scalp EEG, show sizable trial-by-trial variability in response to a given stimulus, as reviewed in Introduction. Local field potentials and firing rates in the cat visual cortex, for example, were reported to oscillate with the peak frequency near 40 Hz in response to the presentation of optimally aligned bars, with randomly varied phases from trial to trial (Gray and Singer, 1989). Also in EEG, the P3, for example, is shown to have variable latencies from condition to condition, which correlate with the time required for stimulus processing and response selection (Verleger, 1997; Verleger et al., 2014). Trial-by-trial variability of response latency may lead to a reduction in the amplitude or even cancellation of an ERP component, potentially leading to an erroneous interpretation of ERP results (Kappenman; Luck, 2014). Even when the amplitude of single-trial response is constant, latency jitter results in a smeared-our version of single-trial response and the reduction in the amplitude of averaged response. If an ERP response contains both positive and negative variations, latency

jitter causes cancellation of the component. It is therefore critical to estimate and compensate trial-by-trial variability of response onsets for correctly interpreting ERP results.

We briefly argue two possible physiological mechanisms of latency jitter. One possible physiological origin of latency jitter is an interaction between an ongoing, spontaneous activity and an event-evoked activity. There is electrophysiological evidence that a single-trial response is the sum of a reproducible response (which is constant over trials) and an ongoing activity (which varies from trial to trial) reported in the cat visual cortex (Arieli et al., 1996). Therefore, depending on the initial state at the moment of stimulus presentation, the response varies due to the different state of ongoing activity, leading to trial-by-trial jitter of activity onsets. Another possible origin is balanced inputs of excitation and inhibition. It is known that, when excitatory and inhibitory inputs are approximately balanced, single-neuron responses exhibit strongly chaotic dynamics even when external inputs are constant (van Vreeswijk and Sompolinsky, 1996). The same mechanism of balanced excitation of inhibition could lead to variable response to a constant input in the model of ERP generation. (Jansen and Rit, 1995). Whereas our method cannot directly answer the physiological mechanisms of trial-by-trial variability, it can be a useful analysis tool to identify and separate reproducible components.

4.4. Limitations and Future Extensions

An assumption of xTRCA is that a TRC is a unit response component, so a trial timing is shifted globally for a whole trial duration. It is known, however, that evoked responses consist of a few separable

components that differ in scalp projections, time-courses, and proposed functions. As a well-established example, P300 during an oddball task is known to consist of at least two components, namely P3a and P3b (Katayama and Polich, 1998; Polich, 2007). P3a lies mainly in the frontal lobe, has an earlier latency (about 380 ms), and is elicited by infrequent novel stimuli, thereby reflecting bottom-up attention. P3b lies mainly in the parietal lobe, has a later time-course (up to 480 ms), and is elicited in a task-relevant manner in relation to memory update. Given their difference, it is conceivable that their latencies could jitter independently, which violates the assumption of unit response. One possible solution is to "time-warp" data using non-linear alignment method (Gupta et al., 1996) so that single-trial data are aligned point-by-point, thus onsets of subcomponents are also aligned. Integrating xTRCA with the recent development of the time-warping method, such as dynamic time warping (DTW) that has been widely used in the field of automatic speech recognition, would be of interest for future studies to address the issue of subcomponents within a TRC.

Another possible extension of xTRCA is to extend the current, offline algorithm to an online one toward possible application of xTRCA to brain-computer interfaces. Our previous method, TRCA, was successfully applied to enhancing the performance of an SSVEP-based speller with the spatial filter that maximized the reproducibility of EEG responses to flickering visual stimuli (Nakanishi et al., 2017). This study has demonstrated, as a proof of concept, an offline analysis that the combination of spatial filter and timing optimization further improved the performance of classification for three-subject data. As noted, most approaches used for brain-computer interfaces use spatial filters only, yet our results indicate that

timing optimization is equally important in the performance improvement. We are currently working on an online extension of xTRCA algorithm for multiple-subject data for more systematic assessment of performance improvement using xTRCA. This extension will be reported in a future study.

The core idea of trial reproducibility maximization can be defined in various features of neuroimaging data. This study defined trial reproducibility in the time domain, thereby leading to a reproducible waveform at every trial. Another study, in contrast, maximized trial reproducibility of the spectrum in the frequency domain to enhance SSVEP responses (Dmochowski et al., 2015). It is straightforward to extend trial reproducibility to the time-frequency domain, and it could be an interesting future direction. We also formulated trial reproducibility in the spatial domain so that scalp topographies of single trials are consistent over trials. By defining the features for trial reproducibility according to a problem in question, the concept of trial reproducibility will find broad applicability for cognitive neuroscience and brain-compute interfaces.

4.3. Conclusion

We developed a cross-correlation trial reproducibility maximization (xTRCA) algorithm to extend possibility of time-domain ERP waveform analysis to induced (i.e. non-phase-locked to stimulus onset) responses. This is an extension of previously published linear spatial filter method, task-related component analysis (TRCA) (Tanaka et al., 2013, 2014) with additional cross-correlation approach to maximize trial-reproducible component (TRC). It is a unified method that fills a gap between analyses of evoked and induced ERPs.

Acknowledgments

We thank Dr. Mike X Cohen for answering our inquiry and providing his Matlab code about simulating scalp EEG by solving the forward model, Dr. Gregory Light for providing the data of mismatch negativity experiment, and Drs. Scott Makeig and Hiroyuki Kambara for helpful discussions and encouragements. We also thank collaborators in Swartz Center for Computational Neuroscience, University of California San Diego for discussions, where a part of this work was conducted. This work is supported by JSPS KAKENHI Grant-in-Aid for Scientific Research (Grant Numbers 25430007, 26120005 and 16K12476), the JSPS Programs (Program for Advancing Strategic International Networks to Accelerate the Circulation of Talented Researcher, and Embodied-Brain Systems Science), and the Hitachi-Kurata and the Tateishi Science Foundations. We acknowledge two anonymous reviewers for providing helpful comments in improving the previous version of the manuscript.

References

Arico P, Aloise F, Schettini F, Salinari S, Mattia D, Cincotti F (2014) Influence of P300 latency jitter on event related potential-based brain-computer interface performance. J Neural Eng 11:035008.

Arieli A, Sterkin A, Grinvald A, Aertsen A (1996) Dynamics of ongoing activity: explanation of the large variability in evoked cortical responses. Science 273:1868-1871.

Artac M, Jogan M, Leonardis A (2002) Incremental PCA for on-line visual learning and recognition. In: Pattern Recognition, 2002. Proceedings. 16th International Conference on, pp 781-784: IEEE.

Benjamini Y, Hochberg Y (1995) Controlling the false discovery rate: a practical and powerful approach to multiple testing. Journal of the royal statistical society Series B (Methodological):289-300.

Blankertz B, Tomioka R, Lemm S, Kawanabe M, Muller K-R (2008) Optimizing spatial filters for robust EEG single-trial analysis. IEEE Signal processing magazine 25:41-56.

Cabasson A, Meste O (2008) Time delay estimation: A new insight into the Woody's method. IEEE signal processing letters 15:573-576.

Clemmensen L, Hastie T, Witten D, Ersbøll B (2011) Sparse discriminant analysis. Technometrics 53:406-413.

Cohen MX (2014) Analyzing neural time series data: theory and practice: MIT Press.

Cohen MX (2017) Comparison of linear spatial filters for identifying oscillatory activity in multichannel data. J Neurosci Methods 278:1-12.

Cohen MX (2018) Using spatiotemporal source separation to identify prominent features in multichannel data without sinusoidal filters. Eur J Neurosci 48:2454-2465.

Congedo M, Korczowski L, Delorme A, Lopes da Silva F (2016) Spatio-temporal common pattern: A

companion method for ERP analysis in the time domain. J Neurosci Methods 267:74-88.

Corsi-Cabrera M, Galindo-Vilchis L, del-Rio-Portilla Y, Arce C, Ramos-Loyo J (2007) Within-subject reliability and inter-session stability of EEG power and coherent activity in women evaluated monthly over nine months. Clin Neurophysiol 118:9-21.

d'Aspremont A, Ghaoui LE, Jordan MI, Lanckriet GR (2005) A direct formulation for sparse PCA using semidefinite programming. In: Advances in neural information processing systems, pp 41-48.

Da Pelo P, De Tommaso M, Monaco A, Stramaglia S, Bellotti R, Tangaro S (2018) Trial latencies estimation of event-related potentials in EEG by means of genetic algorithms. J Neural Eng 15:026016.

Delorme A, Makeig S (2004) EEGLAB: an open source toolbox for analysis of single-trial EEG dynamics including independent component analysis. J Neurosci Methods 134:9-21.

Dmochowski JP, Greaves AS, Norcia AM (2015) Maximally reliable spatial filtering of steady state visual evoked potentials. Neuroimage 109:63-72.

Galambos R (1992) A comparison of certain gamma band (40-Hz) brain rhythms in cat and man. In: Induced rhythms in the brain, pp 201-216: Springer.

Gips B, Bahramisharif A, Lowet E, Roberts MJ, de Weerd P, Jensen O, van der Eerden J (2017) Discovering recurring patterns in electrophysiological recordings. J Neurosci Methods 275:66-79.

Gray CM, Singer W (1989) Stimulus-specific neuronal oscillations in orientation columns of cat visual cortex. Proc Natl Acad Sci U S A 86:1698-1702.

Gupta L, Molfese DL, Tammana R, Simos PG (1996) Nonlinear alignment and averaging for estimating the evoked potential. IEEE Trans Biomed Eng 43:348-356.

Haufe S, Dahne S, Nikulin VV (2014) Dimensionality reduction for the analysis of brain oscillations. Neuroimage 101:583-597.

Huffmeijer R, Bakermans-Kranenburg MJ, Alink LR, van Ijzendoorn MH (2014) Reliability of event-related potentials: the influence of number of trials and electrodes. Physiol Behav 130:13-22.

Jansen BH, Rit VG (1995) Electroencephalogram and visual evoked potential generation in a mathematical model of coupled cortical columns. Biol Cybern 73:357-366.

Jaskowski P, Verleger R (1999) Amplitudes and latencies of single-trial ERP's estimated by a maximum-likelihood method. IEEE Trans Biomed Eng 46:987-993.

Kappenman E S., & Luck, SJ (2012). ERP Components: The ups and downs of brainwave recordings. SJ Luck, Kappenman, & S Emily (Eds), Oxford handbook of event-related potential components:3-30.

Katayama J, Polich J (1998) Stimulus context determines P3a and P3b. Psychophysiology 35:23-33.

Luck SJ (2014) An introduction to the event-related potential technique: MIT press.

Mak JN, Arbel Y, Minett JW, McCane LM, Yuksel B, Ryan D, Thompson D, Bianchi L, Erdogmus D (2011) Optimizing the P300-based brain-computer interface: current status, limitations and future directions. J Neural Eng 8:025003.

Makeig S (1993) Auditory event-related dynamics of the EEG spectrum and effects of exposure to tones. Electroencephalogr Clin Neurophysiol 86:283-293.

Mitra P (2007) Observed brain dynamics: Oxford University Press.

Mowla MR, Huggins JE, Thompson DE (2017) Enhancing P300-BCI performance using latency estimation. Brain Comput Interfaces (Abingdon) 4:137-145.

Mullen TR, Kothe CA, Chi YM, Ojeda A, Kerth T, Makeig S, Jung TP, Cauwenberghs G (2015) Real-

Time Neuroimaging and Cognitive Monitoring Using Wearable Dry EEG. IEEE Trans Biomed Eng 62:2553-2567.

Nakanishi M, Wang Y, Chen X, Wang YT, Gao X, Jung TP (2017) Enhancing Detection of SSVEPs for a High-Speed Brain Speller Using Task-Related Component Analysis. IEEE Trans Biomed Eng.

Ouyang G, Herzmann G, Zhou C, Sommer W (2011) Residue iteration decomposition (RIDE): A new method to separate ERP components on the basis of latency variability in single trials. Psychophysiology 48:1631-1647.

Pekkonen E, Rinne T, Naatanen R (1995) Variability and replicability of the mismatch negativity. Electroencephalogr Clin Neurophysiol 96:546-554.

Polich J (2007) Updating P300: an integrative theory of P3a and P3b. Clin Neurophysiol 118:2128-2148.

Rissling AJ, Braff DL, Swerdlow NR, Hellemann G, Rassovsky Y, Sprock J, Pela M, Light GA (2012) Disentangling early sensory information processing deficits in schizophrenia. Clin Neurophysiol 123:1942-1949.

Rivet B, Souloumiac A, Attina V, Gibert G (2009) xDAWN algorithm to enhance evoked potentials: application to brain-computer interface. IEEE Trans Biomed Eng 56:2035-2043.

Sameni R, Jutten C, Shamsollahi MB (2010) A deflation procedure for subspace decomposition. IEEE Transactions on Signal Processing 58:2363-2374.

Segalowitz SJ, Barnes KL (1993) The reliability of ERP components in the auditory oddball paradigm. Psychophysiology 30:451-459.

Sjöstrand K, Clemmensen LH, Larsen R, Einarsson G, Ersbøll BK (2018) Spasm: A matlab toolbox for sparse statistical modeling. Journal of Statistical Software 84.

Sklare DA, Lynn GE (1984) Latency of the P3 event-related potential: normative aspects and within-subject variability. Electroencephalogr Clin Neurophysiol 59:420-424.

Tadel F, Baillet S, Mosher JC, Pantazis D, Leahy RM (2011) Brainstorm: a user-friendly application for MEG/EEG analysis. Comput Intell Neurosci 2011:879716.

Tanaka H, Katura T, Sato H (2013) Task-related component analysis for functional neuroimaging and application to near-infrared spectroscopy data. Neuroimage 64:308-327.

Tanaka H, Katura T, Sato H (2014) Task-related oxygenation and cerebral blood volume changes estimated from NIRS signals in motor and cognitive tasks. Neuroimage 94:107-119.

Tanaka H, Miyakoshi M, Makeig S (2018) Dynamics of directional tuning and reference frames in humans: A high-density EEG study. Sci Rep 8:8205.

Thompson DE, Warschausky S, Huggins JE (2013) Classifier-based latency estimation: a novel way to estimate and predict BCI accuracy. J Neural Eng 10:016006.

van Vreeswijk C, Sompolinsky H (1996) Chaos in neuronal networks with balanced excitatory and inhibitory activity. Science 274:1724-1726.

Verleger R (1997) On the utility of P3 latency as an index of mental chronometry. Psychophysiology 34:131-156.

Verleger R, Metzner MF, Ouyang G, Smigasiewicz K, Zhou C (2014) Testing the stimulus-to-response bridging function of the oddball-P3 by delayed response signals and residue iteration decomposition (RIDE). Neuroimage 100:271-280.

Weng J, Zhang Y, Hwang W-S (2003) Candid covariance-free incremental principal component analysis. IEEE Transactions on Pattern Analysis and Machine Intelligence 25:1034-1040.

Woody CD (1967) Characterization of an adaptive filter for the analysis of variable latency neuroelectric

signals. Medical and biological engineering 5:539-554.

Zou H, Hastie T, Tibshirani R (2006) Sparse principal component analysis. Journal of computational and graphical statistics 15:265-286.